



HAL
open science

Unravelling functions of halogen substituents in the enantioseparation of dihalogenated ferrocenes on polysaccharide-based chiral stationary phases: experimental and electrostatic potential analyses

Barbara Sechi, Alessandro Dessì, Carlo Gatti, Roberto Dallochio, Bezhan Chankvetadze, Sergio Cossu, Victor Mamane, Patrick Pale, Paola Peluso

► To cite this version:

Barbara Sechi, Alessandro Dessì, Carlo Gatti, Roberto Dallochio, Bezhan Chankvetadze, et al.. Unravelling functions of halogen substituents in the enantioseparation of dihalogenated ferrocenes on polysaccharide-based chiral stationary phases: experimental and electrostatic potential analyses. *Journal of Chromatography A*, In press, 10.1016/j.chroma.2022.463097 . hal-03656876

HAL Id: hal-03656876

<https://hal.science/hal-03656876v1>

Submitted on 2 May 2022

HAL is a multi-disciplinary open access archive for the deposit and dissemination of scientific research documents, whether they are published or not. The documents may come from teaching and research institutions in France or abroad, or from public or private research centers.

L'archive ouverte pluridisciplinaire **HAL**, est destinée au dépôt et à la diffusion de documents scientifiques de niveau recherche, publiés ou non, émanant des établissements d'enseignement et de recherche français ou étrangers, des laboratoires publics ou privés.

Unravelling functions of halogen substituents in the enantioseparation of dihalogenated ferrocenes on polysaccharide-based chiral stationary phases: experimental and electrostatic potential analyses

Barbara Sechi,^{a,‡} Alessandro Dessì,^{a,‡} Carlo Gatti,^b Roberto Dallochio,^a Bezhan Chankvetadze,^c Sergio Cossu,^d Victor Mamane,^{e,*} Patrick Pale,^e and Paola Peluso^{a,*}

^a Istituto di Chimica Biomolecolare ICB, CNR, Sede secondaria di Sassari, Traversa La Crucca 3, Regione Balduca, I-07100 Li Punti - Sassari, Italy

^b CNR-SCITEC, Istituto di Scienze e Tecnologie Chimiche “Giulio Natta”, sezione di via Golgi, via C. Golgi 19, 20133 Milano, Italy

^c Institute of Physical and Analytical Chemistry, School of Exact and Natural Sciences, Tbilisi State University, Chavchavadze Ave 3, 0179 Tbilisi, Georgia

^d Dipartimento di Scienze Molecolari e Nanosistemi DSMN, Università Ca' Foscari Venezia, Via Torino 155, I-30172 Mestre Venezia, Italy

^e Institut de Chimie de Strasbourg, UMR CNRS 7177, Equipe LASYROC, 1 rue Blaise Pascal, 67008 Strasbourg Cedex, France

* Corresponding authors. E-mail address: paola.peluso@cnr.it (Paola Peluso); vmamane@unistra.fr (Victor Mamane)

‡ These authors contributed equally to this work

ABSTRACT

Planar chiral halogenated ferrocenes have come in useful as synthetic intermediates over the years, allowing for the preparation of functionalized derivatives for catalysis, material science, optoelectronics, and medicinal chemistry. Despite their chemical interest, few planar chiral halogenated ferrocenes have been prepared in enantiopure form by asymmetric synthesis so far. Enantioselective HPLC on polysaccharide-based chiral stationary phases (CSPs) has been used for resolving planar chiral ferrocenes making both enantiomers available. However, the enantioseparation of derivatives containing halogens or alkyl groups exclusively remains rather challenging. Given this context, in this study the enantioseparation of eleven planar chiral dihalogenated ferrocenes was systematically explored by using

29 five polysaccharide-based CSPs under multimodal elution conditions. Baseline enantioseparations were
30 achieved for nine analytes with separation factors (α) ranging from 1.20 to 1.44. Thermodynamic
31 quantities associated with the enantioseparations were derived from van't Hoff plots, and for 1-halo-2-
32 (iodoethynyl)ferrocenes (1-halogen = F, Cl, Br) halogen-dependent thermodynamic profiles were
33 identified on a cellulose *tris*(3,5-dimethylphenylcarbamate)-based column. The impact of CSP structure
34 and mobile phase (MP) polarity on the enantioseparation was evaluated. In addition, with the aim to
35 unravel the functions of halogen substituents in mechanisms and noncovalent interactions underlying
36 selector-selectand complex formation at molecular level, local electron charge density of specific
37 molecular regions of the interacting partners were evaluated in terms of calculated electrostatic potential
38 (V) and related source function (SF) contributions. On this basis, the impact of halogen type and position
39 on the enantioseparation was investigated by correlating theoretical and experimental data.

40

41

42

43 *Keywords:* Electrostatic potential, Enantioseparation, Halogen bond, High-performance liquid
44 chromatography, Polysaccharide-based chiral stationary phases, Source function

45

46

47

48 **1. Introduction**

49 The serendipitous discovery of ferrocene in 1951 [1, 2], and its structural determination a year later
50 [3-5], have initiated an ever-increasing number of researches, which have led to the synthesis of
51 numerous substituted ferrocenyl derivatives for various applications, from fuel additive and
52 electrochemistry to catalysis, medicinal chemistry, optoelectronics, and material sciences [6-8].
53 Haloferrocenes were among the first of these derivatives [9], at first in exploratory works but also in
54 attempts to reach the elusive ferrocene, analog to benzyne [10, 11]. Since, halogenated ferrocenes have
55 appeared as key intermediates for accessing polysubstituted ferrocenes [12]. More recently, iodinated
56 ferrocenes turned out to be involved in halogen bond (XB) in solid state [13, 14], and even in solution
57 with emerging application as organocatalyst in organic synthesis [13, 15].

58 Due to the peculiar ferrocene structure, halogenated and other substituted ferrocenes exhibit planar
59 chirality depending on the substitution pattern. Monosubstituted ferrocenes are prochiral compounds,
60 while different disubstitution on one ferrocene ring leads to planar chirality. Such phenomenon has led to
61 the huge development of ferrocenyl derivatives as chiral ligands in asymmetric synthesis and catalysis
62 [8,16]. However, only a few enantiomerically enriched haloferrocenes are known [17-20].

63 Although asymmetric synthesis procedures for accessing enantiomerically enriched halogenated
64 ferrocenes are available, enantiomeric purity is not always satisfactory [21]. An alternative could be the
65 resolution of planar chiral ferrocenes through enantioselective HPLC on polysaccharide-based chiral
66 stationary phases (CSPs). However, while moderate to high enantioselectivities were obtained under
67 normal-phase (NP) elution conditions for ferrocenes bearing polar substituents [19,20,22], the
68 enantioseparation of derivatives containing halogens or alkyl groups exclusively remains rather
69 challenging [23-25].

70 Given the interest in the chemistry of halogenated ferrocenes, and especially of planar chiral ones, we
71 reported herein a systematic study on the HPLC enantioseparability of ferrocenes **1-11** (Fig. 1) by using
72 five polysaccharide-based CSPs (Table S1, Supplementary data) under multimodal elution conditions.

73 For some halogenated ferrocenes, the effect of temperature on the enantioseparations was considered,
74 and thermodynamic quantities associated with the enantioseparations were derived from van't Hoff
75 plots.

76 A second aim of this study was to evaluate the functions of halogen substituents on the
77 enantioseparation [26], exploring the possibility of XB-based enantiorecognition mechanisms [27,28].
78 For this purpose, electrostatic potential values, mapped on electron density isosurfaces (V_s) and
79 associated with the main interaction sites of selectors and of compounds **1–11**, were calculated and
80 correlated with the chromatographic parameters [29]. In addition, with the aim of theoretically
81 explaining the origin and trends of the calculated V values, the source function (SF) reconstruction of V
82 was also applied [30-32]. Recently, this theoretical approach has provided insights into the
83 stereoelectronic features underlying the interaction capability of selectands in LC analyses [31-33].

84 **2. Materials and methods**

85 *2.1. Chemicals*

86 Compounds **1-11** were prepared and characterized as previously reported [15,34-36]. HPLC grade *n*-
87 hexane (Hex), methanol (MeOH), 2-propanol (2-PrOH), and water were purchased from Sigma-Aldrich
88 (Taufkirchen, Germany).

89 *2.2. Chromatography*

90 An Agilent Technologies (Waldbronn, Germany) 1100 Series HPLC system (high-pressure binary
91 gradient system equipped with a diode-array detector operating at multiple wavelengths (220, 254, 280,
92 360 nm), a programmable autosampler with a 20 μ l loop, and a thermostated column compartment) was
93 employed. Data acquisition and analyses were carried out with Agilent Technologies ChemStation
94 Version B.04.03 chromatographic data software. The UV absorbance is reported as milliabsorbance
95 units (mAU). Lux Cellulose-1 (C-1) (cellulose *tris*(3,5-dimethylphenylcarbamate), CDMPC), Lux i-
96 Cellulose-5 (iC-5) (cellulose *tris*(3,5-dichlorophenylcarbamate), CDCPC), Lux Amylose-1 (A-1) and
97 Lux i-Amylose-1 (iA-1) (amylose *tris*(3,5-dimethylphenylcarbamate), ADMPC), and Lux i-Amylose-3

98 (iA-3) (amylose *tris*(3-chloro-5-methylphenylcarbamate), ACMPC) (5 μm) (Phenomenex Inc., Torrance,
99 CA, USA), were used as chiral columns (250 \times 4.6 mm). Analyses were performed in isocratic mode at
100 25°C if not indicated otherwise. The flow rate (*FR*) was set at 0.8 ml/min. For compounds **1**, **3**, and **6**,
101 the enantiomer elution order (EEO) was determined by injecting enantiomers of known absolute
102 configuration [15]. For compounds **2**, **4**, **5**, and **7-11**, the relative EEO was assigned by injecting pure
103 enantiomers of unknown absolute configuration which are denoted as $X_{\text{compound number}}$ and $Y_{\text{compound number}}$.
104 The van't Hoff experiments were conducted at 5, 10, 15, 20, 25, 30, 35, and 40 °C by using a thermostat
105 jacket equipped with a RE104 LAUDA circulating water-bath (Lauda, Königshofen, Germany)
106 (resolution 0.1 °C; accuracy ± 0.4 °C; temperature control ± 0.02 °C). When the temperature was
107 changed, the column was allowed to equilibrate for 1 h before injecting the samples. Thermodynamic
108 parameters were derived from the slopes and the intercepts of the van't Hoff plots by linear regression
109 analysis (see Supplementary data for details). Statgraphics Centurion XVI (Statpoint Technologies, Inc.,
110 Warrenton, VA, USA) was used for all linear regression analyses.

111 2.3. Computations

112 Electrostatic potential extrema on the molecular electron density isosurfaces (maxima and minima)
113 ($V_{S,\text{max}}$ and $V_{S,\text{min}}$) (au, electrons/bohr) were calculated by using Gaussian 09 (Wallingford, CT 06492
114 USA) [37], at the density functional theory (DFT) level of theory using the B3LYP functional and the
115 def2TZVPP basis set. Search for the exact location of $V_{S,\text{max}}$ and $V_{S,\text{min}}$ was made through the Multiwfn
116 code [38] and through its module enabling quantitative analyses of molecular surfaces (isovalue 0.002
117 au) [39]. Theory and details of the SF reconstruction of V_S are available in the Supplementary data. The
118 results of the SF decomposition of $V_{S,\text{extrema}}$ are described on the basis of the equations (1,2) for
119 compounds **1-6** and **7-11**, respectively, with X = F, Cl, Br and Cp = cyclopentadienyl.

$$120 \quad V_{S,\text{extrema}} = \text{SF}(\text{I}) + \text{SF}(\text{X}) + \text{SF}(\text{Fe}) + \text{SF}(\text{C}\equiv\text{C}) + \text{SF}(\text{Cp}_{\text{substituted}}) + \text{SF}(\text{Cp}_{\text{unsubstituted}}) \quad (1)$$

$$121 \quad V_{S,\text{extrema}} = \text{SF}(\text{I}) + \text{SF}(\text{X}) + \text{SF}(\text{Fe}) + \text{SF}(\text{Cp}_{\text{substituted}}) + \text{SF}(\text{Cp}_{\text{unsubstituted}}) \quad (2)$$

122

123 3. Results and discussion

124 3.1. Conceptual basis: integrating experimental and electrostatic potential analyses

125 With the twofold purpose of *i*) improving methods to enantioseparate halogenated ferrocenes, and *ii*)
126 unravelling enantioseparation mechanisms at the molecular level, the impact of analytes and CSP
127 structures, and of mobile phase (MP) polarity on retention (*k*) and separation (α) factors was explored.
128 Thus, CSPs, and MPs and analytes were selected on the basis of the following remarks:

129 *a*) the performances of different polysaccharide selectors were evaluated, and compared in terms of
130 polysaccharide backbone (cellulose-based C-1 vs. amylose-based A-1), and of type of carbamate
131 pendant groups (methylated A-1, iA-1, C-1 vs. chlorinated iC-5 vs. methylated and chlorinated iA-3)
132 (Table S1, Supplementary data). The electronic properties of the carbamate moiety, which are tuned by
133 methyl and chlorine substituents located on the phenyl ring of the carbamate pendant groups, were
134 determined by DFT calculations (Table S2, Supplementary data). The impact of the anchoring technique
135 (immobilization vs. coating) was also considered by comparing the performances of amylose *tris*(3,5-
136 dimethylphenylcarbamate) (ADMPC)-based columns (A-1 *versus* iA-1) [40,41];

137 *b*) under multimodal elution conditions, the effect of MP on the enantioseparations was comparatively
138 evaluated by using Hex/2-PrOH 95:5 v/v (A), Hex/2-PrOH/MeOH 95:2.5:2.5 v/v/v (B), MeOH 100%
139 (C), MeOH/water 95:5 v/v (D), and MeOH/water 90:10 v/v (E). In particular, the comparative use of A-
140 E, as MPs, allowed for evaluating the effect of increasing hydrophobicity of the medium. Indeed,
141 recently, methanol-containing MPs were shown to favour the enantioseparation of non-polar ferrocenes
142 [26]. The use of pure MeOH (C) impacts the intramolecular hydrogen bonds (HBs) determining the
143 highly-ordered structure of the polysaccharide, thus producing a huge effect within the polysaccharide
144 structure [42-44]. With MeOH, hydrophobic interactions tend to be more favoured compared to HBs,
145 and the addition of water was expected to enhance hydrophobic interactions and increase capacity
146 factors in accordance with a typical reversed-phase (RP) system [45]. In contrast, 2.5% MeOH (B) does
147 not affect the highly-ordered three-dimensional structure of the polysaccharide. Rather, it may allow for

148 fine tuning of the binding between analyte and polysaccharide-based selector by favouring a better
149 penetration of the analyte into the groove, and modulating hydrophobic *versus* HB interactions [42,43].
150 As ferrocene may be considered a three-dimensional analogue of the flat benzene ring [23], and its
151 “barrel shape” offers better possibility for filling hydrophobic cavities compared to aryl and heteroaryl
152 rings [46]. Indeed, methanol-containing MPs were shown to favour the enantioseparation of non-polar
153 ferrocenes [25].

154 *c)* within the 1-halo-2-iodoethynyl (**1-3**), 1-halo-3-iodoethynyl (**4-6**), 1-halo-2-iodo (**7-9**), and 1-halo-
155 3-iodo (**10,11**) ferrocene series (Fig. 1), the impact on enantioseparation of the substitution pattern (1,2-
156 disubstituted: **1-3**, **7-9** vs 1,3-disubstituted: **4-6**, **10**, **11**), of the C≡C framework (**1-6** vs **7-11**), and of the
157 distinctive halogen atom (F: **1**, **4**, **7**, **10**; Cl: **2**, **5**, **8**, **11**; Br: **3**, **6**, **9**) was evaluated. In compounds **1-11**,
158 bound halogens may behave as (Fig. 2) *a)* HB and XB acceptors (I < Br < Cl < F) through the region of
159 higher electron density, which forms a belt orthogonal to the C–X covalent bond, *b)* XB donor (I > Br >
160 Cl > F) through the region of electron charge density depletion (σ -hole) located on the elongation of the
161 C–X covalent bond, *c)* hydrophobic centres (I > Br > Cl > F), and *d)* bulky groups participating in
162 repulsive interactions, in particular the heavy halogens such as Br (radius = 1.85 Å [47]) and I (radius =
163 1.98 Å [47]). In addition, the C≡C electronic cloud may function as HB acceptor, and the ferrocene Cp
164 π -clouds have also electron donor properties.

165 With the aim of exploring the interaction capability of compounds **1-11**, the local electron charge
166 density of specific molecular regions of the analytes was investigated in terms of calculated V_S extrema,
167 $V_{S,max}$ and $V_{S,min}$ (Fig. 2 and Table S3, Supplementary data), which are associated with electrophilic and
168 nucleophilic regions, respectively. Moreover, the $V_{S,max}$ and $V_{S,min}$ values may be envisaged as being due
169 to SF contributions from atoms or groups of the system by extending the Bader–Gatti SF for the electron
170 density to V , as previously reported [31-33,48]. Thus, the decomposition of V in atomic or group
171 contributions was considered in order to quantify the impact of single contributions to the V value
172 (Tables S4-S13, Supplementary data). On this basis, the factors determining a certain V in a point could

173 be inspected, attempting to disclose the fine reasons at the molecular level of the observed
174 chromatographic trends in series of structurally related compounds. It is reasonable to hypothesize that
175 distinct molecular points may behave differently in noncovalent interactions if they present different SF
176 contribution patterns, even if they also present similar V values at these points. Indeed, different SF
177 contributions may reveal different capabilities of the overall molecule to rearrange electron charge
178 density, stabilizing/destabilizing the system, after the perturbation of the electron charge density in a
179 point due to the noncovalent contact. The source sign associated with $V_{S,max}$ contribution is positive or
180 negative whether the atomic (or group) source concurs or opposes to the positive potential, whereas the
181 opposite occurs for the $V_{S,min}$ contributions.

182 3.2. Chromatographic screening

183 The enantioseparation of the halogenated analytes **1-11** was examined by using twenty-five
184 chromatographic systems generated by the combination of C-1, iC-5, A-1, iA-1, and iA-3, as CSPs, with
185 A-E as MPs (Tables S14-S24, Supplementary data). A-1 and iA-3 showed better enantioseparation
186 versatility toward ferrocenes **1-11** compared to C-1, iC-5 and iA-1, and seven and five compounds could
187 be baseline resolved on these two columns, respectively. On the contrary, iC-5 exclusively provided
188 partial enantioseparation of compound **1**, with low selectivity factors under normal phase (NP) elution
189 conditions (A: $\alpha = 1.09$; B: $\alpha = 1.06$) (Table S14, Supplementary data). The immobilized iA-1 also
190 showed limited versatility, and it could only baseline enantioseparate compounds **10** and **11** by using
191 methanol-containing MPs (**10**: B-E; **11**: D, E). For this series of enantioseparations (Tables S23 and
192 S24), iA1 provided lower selectivity factors ($1.19 \leq \alpha \leq 1.24$) compared to those observed on the coated
193 A1 ($1.37 \leq \alpha \leq 1.42$). As an exception, compound **10** was enantioseparated on iA1 by using mixture B,
194 as MP, whereas it remained not separated on the coated A-1 under the same elution conditions. For the
195 enantioseparations on A-1 and iA-3, the values of k and α are summarized in Figures 3 and 4,
196 respectively, along with the data related to the enantioseparations on C-1, as reference term for
197 comparison.

198 Baseline enantioseparations were obtained at 25 °C for compounds **1-6**, **10**, and **11** with α values
199 ranging from 1.20 to 1.44, whereas the best partial enantioseparations were obtained for **7** ($\alpha = 1.09$), **8**
200 ($\alpha = 1.09$) and **9** ($\alpha = 1.07$) by using the systems iA-3/B, C-1/E, and C-1/A, respectively. In all cases, the
201 best selectivity values were obtained by using A-1 and iA-3 as CSPs with methanol-containing MPs,
202 with the exception of compounds **8** and **9** which showed better enantioseparation on C-1. Compound **3**
203 could be also baseline enantioseparated by using C-1 with mixture A as MP, but with a lower selectivity
204 factor ($\alpha = 1.16$) compared to that obtained with the system A-1/E ($\alpha = 1.21$). Given that temperature
205 impacts the chromatographic behaviour of the analytes in HPLC enantioseparation, it was considered as
206 a variable to optimize separation [41,49,50], and the dependence of the enantioseparation on the
207 temperature was also explored. On this basis, baseline enantioseparations could be also achieved for
208 compound **8** with the system C1/E at 5 °C ($\alpha_{25^\circ\text{C}} = 1.09 \rightarrow \alpha_{5^\circ\text{C}} = 1.22$). Enantioseparation was also
209 improved for **7** ($\alpha = 1.12$) and **9** ($\alpha = 1.13$) by using C-1 at 5 °C with the mixtures A and E, respectively.
210 Nevertheless, baseline enantioseparations were not obtained in both cases. For compound **3**, selectivity
211 with the system A-1/E could be improved by changing the operative temperature from 25 °C ($\alpha = 1.21$)
212 to 10 °C ($\alpha = 1.30$) (Fig. S1, Supplementary data).

213 Several cases of enantiomer elution order (EEO) reversal could be observed (Table 1), which are
214 dependent on polymer backbone (**5**, **6**, **7**: C-1/B \rightarrow A-1/B), pendant groups (**1**: C-1/A \rightarrow iC-5/A; **1**, **3**:
215 A1/E \rightarrow iA-3/E), MP (**2**: C-1/B \rightarrow C-1/E; **8**, **9**: C-1/A \rightarrow C-1/D,E) and distinctive halogen type (C-1/A:
216 **1** \rightarrow **3**) and position (A-1/C,D,E: **3** \rightarrow **6**) in the analyte. No reversal of the EEO was observed for
217 compounds **4**, **10**, and **11**.

218 3.3. Effect of the selector structure on the enantioseparation

219 The columns used in this study contain selectors based on amylose and cellulose backbones. The latter
220 are derivatized with chloro- or/and methyl-substituted phenylcarbamate pendant groups determining the
221 distinctive stereoelectronic properties of each selector (Table S1, Supplementary data,) [40]. The
222 amylose-based columns provided baseline enantioseparation for eight compounds (**1-6**, **10**, **11**), whereas

223 only two compounds (**3**, **8**) were baseline enantioseparated with cellulose-based selectors. The column
224 performances, in terms of number of baseline enantioseparations, decreased following the order A-1 (7)
225 > iA-3 (5) > C-1 (2) > iC-5 (0). Two factors could contribute to this trend:

226 *a) chiral cavity size:* amylose-based selectors present a more compact structure with respect to the
227 cellulose-based selectors [51]. Moreover, the introduction of chlorine increases the fraction of free N–H
228 groups available for selector-analyte interactions [43], whereas the fraction of N–H involved in
229 intramolecular HBs, contributing to maintain the highly-ordered structure of the CSP, decreases. This
230 could produce for the chlorinated CSPs (iC-5 and iA-3) a wider cavity with respect to the dimethylated
231 selectors, the overall enantioseparation resulting from the balance of carbamate polarity and
232 intramolecular HB ability [43]. Thus, the dimension of the cavities inside the groove may be supposed to
233 increase following the order A-1 < iA-3 < C-1 < iC-5. Consequently, more compact chiral cavities
234 defined a better stereochemical environment for the enantio-recognition of halogenated ferrocenes **1-11**,
235 favouring their enantioseparation, likely due to the small size of these ferrocene derivatives ($199 \leq$
236 volume (\AA^3) ≤ 240). Selectivity values for baseline enantioseparations were generally higher for A-1
237 ($1.15 \leq \alpha \leq 1.66$) compared to iA-3 ($1.10 \leq \alpha \leq 1.41$).

238 *b) pendant group structure:* the effect of introducing chlorine in the CSP structure is to modify the
239 electron charge density distribution on the pendant groups, thus the electron charge density on both C=O
240 and phenyl ring decreases (π -acidity increases), whereas the acidity of the N–H increases [43,51].
241 Calculating $V_{S,\max}$ and $V_{S,\min}$ values on the amidic hydrogen and the carbonyl oxygen, respectively,
242 located in the pendant groups of ADMPC (CDMPC) (C-1, A-1, iA-1), CDCPC (iC-5), and ACMPC (iA-
243 3) confirmed this trend (Table S2, Supplementary data). Indeed, the $V_{S,\max}$ and $V_{S,\min}$ decreased
244 following the order CDCPC (0.0990, -0.0536 au) > ACMPC (0.0914, -0.0595 au) > ADMPC (CDMPC)
245 (0.0843, -0.0625). On this basis, given the higher performances of the ADMPC and CDMPC compared
246 to the ACMPC and CDCPC, respectively, the carbonyl oxygens seem to be important recognition sites
247 for the ferrocene derivatives under investigation.

248 In almost all cases iA-1 showed lower enantioseparation ability compared to the coated A-1, thus the
249 immobilization of the selector impacted on the column performances toward ferrocene **1-11**. The
250 immobilized column exhibited good enantioseparation capability for compounds **10** and **11** exclusively,
251 with methanol-containing MPs, thus under hydrophobic conditions. In this regard, it is worth mentioning
252 that all the immobilization conditions produce chemical and/or physical alteration of the selector, and
253 sometimes covalent immobilization technologies require the use of under-derivatized polysaccharides in
254 order to attach the selector to the silica surface [40]. On the other hand, previous studies demonstrated
255 that immobilization of ADMPC could impact the carbamate region, which is involved in HB interactions
256 with the analytes, more than the substituted aromatic rings [41].

257 With the aim to compare the thermodynamic profiles of ADMPC, ACMPC, and CDMPC as selectors
258 contained in A-1, iA-3, and C-1, respectively, by using mixture E as MP, temperature dependence of
259 retention and selectivity was profiled for **1-6**, as representative compounds, in the range 5-40 °C (Tables
260 S25-S34, Figs. S2-S7, Supplementary data). Thermodynamic quantities associated with the adsorption
261 of analytes on the CSP surface were calculated from van't Hoff equations (Supplementary data for
262 details). In this regard, it is worth highlighting that this type of analysis may be useful to inspect the
263 nature of analyte/CSP association on the basis of thermodynamic considerations, but it does not allow
264 for determining individually achiral and chiral features of enantioseparation and their actual ratio in the
265 discrimination [52]. By using the thermodynamic ratio $Q = \Delta\Delta H^\circ / (298 \times \Delta\Delta S^\circ)$ [53] as a parameter for
266 comparison, the thermodynamic analysis evidenced in almost all cases an enthalpic contribution ($\Delta\Delta H^\circ$)
267 to the free energy difference ($\Delta\Delta G^\circ$) associated to the enantioseparation increasing following the order
268 C-1 ($1.00 \leq Q \leq 1.26$) (Table S28) < iA-3 ($1.09 \leq Q \leq 1.70$) (Table S34) < A-1 ($1.17 \leq Q \leq 1.54$) (Table
269 S30 and Fig. S7 for comparative entropy-enthalpy compensation graphs). It is worth noting that the
270 enantioseparations of compounds **1-6** with the systems C-1/A, C-1/E, A-1/E, iA-1/E, and iA-3
271 considered in the thermodynamic analysis were found to be enthalpy-driven in all cases ($Q > 1$) with the
272 exception of the enantioseparation of compounds **1** and **2** with the system C-1/A, showing respectively

273 entropy-driven ($Q < 1$) and mixed enthalpy/entropy-driven profiles (Fig. 5). For compounds **5** and **6**
274 (compounds **1-3** were not enantioseparated with this column), the immobilized iA-1 showed lower Q
275 values ($Q = 1.04, 1.29$) compared to the coated A-1 ($Q = 1.37, 1.54$).

276 As mentioned above, CSP backbone-dependent reversals of EEO was observed for compounds **5**, **6**
277 and **7** by using mixture B as MP, moving from C-1 to A-1. In this case, it is likely that the size of both
278 analytes and selector chiral cavities plays a role, **5** and **6** being the largest compounds of the ferrocene
279 series (volume = 235.63 and 240.16 Å³, respectively), and **7** the smallest (volume = 198.27 Å³).
280 Differently, for compound **1**, a EEO reversal dependent on the CSP pendant group was observed under
281 NP elution conditions (A) moving from C-1 (*R-S*) to iC-5 (*S-R*), and for compounds **1** and **3** in the
282 aqueous methanol mixture E moving from A-1 (*S-R*) to iA-3 (*R-S*). In these cases, the balance between
283 HBs, XBs and hydrophobic interactions could also play a role.

284 3.4. Effect of the mobile phase on the enantioseparation

285 The shape of the curves reported in Figures 3 and 4 suggested the presence of two sets of interactions
286 underlying polar and hydrophobic mechanisms occurring respectively in hexane-based mixtures (A, B)
287 and in aqueous mixtures (D, E). The impact of MP polarity on retention and selectivity appeared to be
288 strictly dependent on analyte and CSP structures. The following trends could be observed:

289 *a)* in several cases, the use of pure MeOH as MP was detrimental for both polar and hydrophobic
290 mechanisms, and V-shaped curves centred on mixture C were obtained in these cases (Figs. 3a,b,c,d,g,h,j
291 and 4a,c,d,g);

292 *b)* MeOH, as a protic solvent, may participate in HBs with chiral selector, as well as with chiral
293 analyte, thus, in some cases application of this solvent was detrimental for analyte-selector polar
294 interactions resulting in decreased retention and selectivity moving from mixture A to B and C (Figs.
295 3a,b,d,e,g,h,j and 4a,d,g);

296 *c*) in other cases, the addition of few percentages of MeOH (B) tended to increase retention and
297 selectivity, likely favouring a better penetration of the analyte into the chiral groove (Figs. 3c,e,f,i,k,l and
298 4a,c-f,h,i,k,l);

299 *d*) the addition of water to methanol showed a variable impact on the enantioseparation depending on
300 analyte and CSP structure.

301 The thermodynamic differences between mixture A and E, in term of Q , were evaluated for column
302 C-1 and compounds **1-6**, showing a general increase of the $\Delta\Delta H^\circ$ contribution to the $\Delta\Delta G^\circ$ moving from
303 the hexane-based mixture ($1.00 \leq Q \leq 1.26$) to the aqueous methanol mixture ($1.17 \leq Q \leq 1.54$).

304 3.5. Impact of analyte structure on the enantioseparation

305 With the aim to evaluate the impact of the substitution pattern (1,2 vs 1,3), of the C≡C framework (–X
306 vs C≡C–X), and of the distinctive halogen type (F, Cl, Br) on the enantioseparability of compounds **1-**
307 **11**, the rate of baseline enantioseparations (*rb*s) at 25 °C was determined from the wealth of
308 chromatographic results. In the frame of the twenty-five chromatographic systems explored in this study
309 at 25°C, the *rb*s decreased following the order **10** (44%) > **11** (36%) > **5** (28%) > **6** (24%) > **4** (16%) >
310 **1,2** (12%) > **3** (8%) > **7-9** (0%). From this trend, some remarks emerged:

311 *a*) 1,3-disubstituted ferrocenes showed higher enantioseparability, in terms of *rb*s, compared to the
312 1,2-disubstituted analogues (**4-6** > **1-3** and **10,11** > **7-9**). Retention factors of **4-6** ($0.03 \leq k \leq 5.63$) and
313 **10,11** ($0.15 \leq k \leq 2.90$) were, in general, higher than those of **1-3** ($0.03 \leq k \leq 1.76$) and **7-9** ($0.14 \leq k \leq$
314 1.83), respectively. As first consideration, in the 1,3-disubstituted series more positive $V_{S,max}$ values
315 ($0.0466 \text{ au} \leq V_{S,max} \leq 0.0738 \text{ au}$) were calculated for the electrophilic σ -holes on halogens compared to
316 the 1,2-disubstituted ferrocenes ($0.0465 \text{ au} \leq V_{S,max} \leq 0.0721 \text{ au}$). In addition, both substituents are fully
317 accessible to the selector in 1,3-disubstituted compounds, whereas the substituents are sterically
318 constrained in 1,2-disubstituted derivatives. In the latter case, through-space contacts of adjacent
319 electron charge density regions [31], associated with the main interaction sites, may contribute to limit
320 the recognizability of the two enantiomers of the planar chiral ferrocenes. This structural feature could

321 be confirmed by the fact that, in general, the SF percentage contribution to a V_S value from adjacent
322 groups of the same type was higher for 1,2-disubstituted compounds compared to the 1,3-disubstituted.
323 ones For instance, in compound **3**, the negative SF percentage contribution of the 2-iodoethynyl
324 framework to the $V_{S,max}$ associated with the σ -hole of the 1-bromine atom is more negative (SF(I) +
325 SF(C \equiv C) = -59.04%) compared to the same type of SF contribution calculated for 1,3-disubstituted
326 ferrocene **6** (SF(I) + SF(C \equiv C) = -32.08%) (Table S9, Supplementary data). The same trend was
327 observed for the SF(I) + SF(C \equiv C) values calculated for the pair **2** (-87.8%) and **5** (48.13%) (X = Cl),
328 whereas a more positive contribution was determined for **1** (70.34%) compared to **4** (51.1%) (X = F).
329 With the aim to understand correctly the meaning of the SF reconstruction, it is worth stressing that the
330 SF contribution to the V in a point \mathbf{r} depends on the electronic features of the contributing atom or
331 groups as well as on the relative position between the contributing framework and the point \mathbf{r} [31]. In
332 addition, the sign of each contribution derives from the balance between nuclear and electronic
333 contribution. In addition, it is interesting to note the opposite contribution sign induced by the presence
334 of the fluorine substituent (**1** and **4**) compared to the chlorinated (**2** and **5**) and brominated (**3** and **6**)
335 compounds. On the basis of these differences, different chromatographic behaviours were expected for
336 the fluorinated compounds compared to the chlorinated and brominated analogues.

337 Given that, compounds **1-3** provided baseline enantioseparations with higher α values ($1.21 \leq \alpha \leq$
338 1.56) compared to compounds **4-6** ($1.10 \leq \alpha \leq 1.44$) on amylose-based CSPs. In these cases, it is likely
339 that the more compact structure of 1,2-disubstituted ferrocenes may penetrate more easily in the compact
340 chiral cavity of amylose-based selectors compared to the bigger 1,3-disubstituted ferrocenes. Moreover,
341 in terms of HB acceptor properties, the $V_{S,min}$ associated with the ethynyl cloud is lower for compounds
342 **1-3** ($-0.0309 \text{ au} \leq V_{S,min} \leq -0.0327 \text{ au}$) compared to **4-6** ($-0.0258 \text{ au} \leq V_{S,min} \leq -0.0266 \text{ au}$). The case of
343 compound **8** proved also to be interesting due to the overlap between $V_{S,min}$ regions which are located in
344 the negative belts of 1-chlorine and 2-iodine substituents of the ferrocenyl unit. This feature generates a
345 region with a lower $V_{S,min}$ value ($V_{S,min} = -0.0251 \text{ au}$) (Supplementary data, Table S3) compared to the

346 nucleophilic regions on the halogens in the analogues **7** ($V_{S,\min} = -0.0109$ au) and **9** ($V_{S,\min} = -0.0113$ au).
347 This feature may justify the fact that **8** could be baseline enantio-separated, whereas partial
348 enantio-separation was only achieved for **7** and **9**. The higher impact of 2-iodine atom on the adjacent 1-
349 chlorine atom could be confirmed considering the SF contribution of iodine to the distinctive $V_{S,\min}$ on
350 halogens, which is more negative for **8** (SF(I) = -121.46%) compared to those of **11** (SF(I) = -68.72%), **7**
351 (SF(I) = -72.70%) and **9** (SF(I) = -120.70%);

352 *b)* the ethynyl framework represents a key structural element which could exert a steric and an
353 electronic impact on enantio-separation. The ethynyl π -cloud is a HB acceptor which may participate in
354 HB with the amidic hydrogen of the selector and, as an EWG group, it activates the iodine σ -hole as
355 electrophile. On the other hand, it induces a larger volume to the 1,3-disubstituted ferrocenes compared
356 to the 1,2-disubstituted analogues. On this basis, the higher enantio-separability of compounds **1-3** ($8\% \leq$
357 $rb_s \leq 12\%$) compared to **7-9** ($rb_s = 0\%$) could be explained in terms of $V_{S,\max}$ values associated to the
358 electrophilic σ -hole on iodine. Indeed, the ethynyl group in **1-3** contributes to increase the electrophilic
359 character of the iodine (0.0720 au $\leq V_{S,\max}(\text{I}) \leq 0.0721$ au) compared to the analogues **7-9** (0.0465 au \leq
360 $V_{S,\max}(\text{I}) \leq 0.0476$ au). However, the opposite trend was observed for the 1,3-substituted derivatives **10**
361 and **11** showing higher enantio-separability compared to **4** and **5**, respectively. In this case, the ethynyl
362 framework could exert a detrimental effect on enantio-separability of **4** and **5**, in particular on iA-1, due
363 to steric reasons;

364 *c)* the Cp system contributes to the hydrophobic character of the overall molecular system featured in
365 compounds **1-11**, and it has also electron donor properties. However, functions of the Cp system at the
366 molecular level are strongly modulated by the distinctive substitution of the ferrocenyl unit. In terms of
367 V (Table S3, Supplementary data), the $V_{S,\min}$ values in the unsubstituted Cp increase following the order
368 $F < Cl < Br$ and **1-3** $<$ **4-6** \approx **2-8** $<$ **10,11**. For the substituted Cp ring, the variations related to halogen
369 type are less important in terms of V variations, whereas, in this case, the $V_{S,\min}$ values increase
370 following the order **1-3** $<$ **7-9** $<$ **4-6** $<$ **10,11**. Moreover, as shown in Table S13, the SF contribution of

371 the distinctive halogens (X) to the $V_{S,\min}$ associated to the Cp π -clouds is strongly type- and position-
372 dependent for both substituted and unsubstituted Cp rings. In turn, the Cp system contribution to the
373 halogen V values is variable in terms of sign and amount, also in this case depending on halogen type
374 and position (Table S4-S12);

375 *d)* as shown in Figures 3 and 4, the impact of halogen type on the enantioseparation may be not easy
376 to rationalize because the fine impact of CSP structure, MP polarity, and the other structural components
377 of the analyte on the enantioseparation, as summarized above, is subtly dependent on steric and
378 electronic properties, and position of F, Cl, and Br as distinctive substituents of compounds **1-11**.
379 However, some hypotheses can be attempted on the basis of the comparative analyses of distinctive
380 results.

381 *3.5.1. Impact of halogen type on the enantioseparation*

382 In most cases, retention of the analyte follows the order $F < Cl < Br$. This observation shows that the
383 electrophilic features of the halogen or its hydrophobic character may drive retention. However, the
384 higher electronegativity of fluorine proved to play a role in some cases. As mentioned above, the iC-5
385 enantioseparated compound **1**, exclusively by using A as MP. This result clearly relates this unique
386 enantioseparation to the complementarity, in terms of HB recognition sites, between the CDCPC and **1**.
387 Indeed, the amidic hydrogen of the CDCPC presents the highest $V_{S,\max}$ value (0.0990 au) among the
388 selectors used in this study, namely the best properties as HB donor (Table S2), and compound **1**
389 features the most negative $V_{S,\min}$ (-0.0347 au) observed in compounds **1-11** (Table S3).

390 The impact of the high electron density of fluorine may be also observed in the enantioseparation of
391 compounds **7-9** with the system A-1/B. In this case the selectivity factor decreases following the order F
392 ($\alpha = 1.10$) > Cl ($\alpha = 1.05$) > Br ($\alpha = 1.00$). However, it is worth noting that, in particular on the amylose-
393 based CSPs, the trend $F > Cl > Br$ could be related to the steric hindrance of the halogens, increasing in
394 the opposite order $Br > Cl > F$. Indeed, the smaller fluorinated compounds should penetrate more easily
395 into the chiral cavities than its larger analogues.

396 An interesting trend emerges from the comparison of the impact of adding 2.5% MeOH in the
397 hexane/2-PrOH mixture A, obtaining the ternary mixture B, on the enantioseparation of compounds **1-3**
398 by using C-1. While for all compounds, retention decreased by adding 2.5% MeOH, the variations in
399 terms of selectivity factors were different. Indeed, α increased for compounds **1** ($\alpha_A = 1.06 \rightarrow \alpha_B = 1.08$)
400 and **2** ($\alpha_A = 1.00 \rightarrow \alpha_B = 1.07$), whereas it decreased for compound **3** ($\alpha_A = 1.16 \rightarrow \alpha_B = 1.00$).
401 Moreover, as mentioned above a reversal of EEO dependent on halogen type could be observed between
402 **1** (*R-S*) and **3** (*S-R*) with the system C1/A. As this trend revealed that diverse mechanisms could underlie
403 retention and selectivity, we evaluated comparatively the thermodynamic profiles of compounds **1-3** in
404 the range 5-40°C, with the chromatographic system C-1/A (Fig. 5). For compounds **1-3**, the T_{ISO} were
405 calculated from the thermodynamic quantities determined by classical van't Hoff equations as 7°C, 35°C
406 and 69°C. At the T_{ISO} , the $\Delta\Delta H^\circ$ and $\Delta\Delta S^\circ$ terms contributing to the free energy difference ($\Delta\Delta G^\circ$)
407 compensate each other, the free energy term is zero and the enantiomers co-elute. In general,
408 enantioseparations at lower temperatures than T_{ISO} are enthalpy-driven ($|\Delta H^\circ| > |T\Delta S^\circ|$), whereas at
409 higher temperatures enantioseparations are entropy-driven ($|\Delta H^\circ| < |T\Delta S^\circ|$). By changing the temperature
410 between the two regions, an EEO reversal occurs. On this basis, the thermodynamic profile of the
411 enantioseparation resulted entropic for compound **1**, containing F as distinctive halogen (Fig. 5a),
412 enthalpic for **3** (X = Br) (Fig. 5c), and a mixed entropic/enthalpic behaviour was obtained for **2** (X = Cl)
413 (Fig. 5b). For this latter enantioseparation, the EEO in the enthalpic domain was Y_2-X_2 . In this regard,
414 with the aim to verify the chromatographic behaviour in the region of the entropy domain, the
415 enantioseparation of compound **2** was also performed at 45°C. Partial separation was observed at this
416 temperature with the expected reversal of EEO (X_2-Y_2). For the structurally related compounds **1** and **3**,
417 reversal of EEO was associated with two opposite thermodynamic profiles, *R-S* (**1**) in the entropy-driven
418 domain, and *S-R* (**3**) in the enthalpy-driven domain. On this basis, due to its structural similarity to
419 compounds **1** and **3**, for compound **2** it was reasonable to assign *S-R* to the undefined Y_2-X_2 in the
420 enthalpic domain, and *R-S* to X_2-Y_2 in the entropic domain (Table 1). With the aim of identifying the

421 distinctive recognition sites which produced different mechanisms at the molecular level, despite the
422 similarity of the three compounds, $V_{S,\min}$ and $V_{S,\max}$ values on halogens were evaluated and compared. In
423 this regard, V analysis showed that no relevant difference could be observed in compounds **1-3** in terms
424 of V values of the cyclopentadienyl rings, iodine σ -holes and electronegative belts (Fig. 5d-f). Rather, 1-
425 halogen atoms present major differences in terms of σ -hole and electronegative belt. Indeed, the σ -hole
426 $V_{S,\max}$ increases following the order $F < Cl < Br$ as the polarizability of the halogens, whereas the $V_{S,\min}$
427 on the halogen belt increases following the opposite order $Br < Cl < F$. Given that, the fluorine atom in
428 compound **1** has higher electron density with a negative value of both $V_{S,\min}$ (-0.0347 au) and $V_{S,\max}$ (-
429 0.0249 au) (Fig. 5d). Otherwise, the bromine atom, in compound **3**, has a more positive $V_{S,\max}$ (0.0291
430 au) and a less negative $V_{S,\min}$ (-0.0156 au) (Fig. 5f) compared to the chlorine atom in compound **2**, which
431 presents intermediate values for chlorine $V_{S,\min}$ (-0.0163 au) and $V_{S,\max}$ (0.0189 au) (Fig. 5e). On this
432 basis, it can be reasonably expected that HB involving the NH group of the selector as the HB donor
433 participates in the enantiodifferentiation mechanism for the fluorinated compound **1**, whereas XB
434 involving the carbonyl group of the selector for the more polarizable 1-bromo substituted compound **3**.
435 Reasonably, in the first case, increasing temperature favours accommodation of the analyte into the
436 groove, and the formation of the strong $N-H\cdots F-Fc$ ($Fc = ferrocene$) noncovalent interaction. In parallel,
437 after complex formation, the entropy of the system increases, likely due to desolvation phenomena
438 related to the binding sites and to the hydrophobic feature of the analyte ($\Delta\Delta S^\circ = 1.93$, $Q = 0.94$; EEO =
439 R - S). In the case of compound **3**, given the higher positive $V_{S,\max}$ on the bromine σ -hole, the
440 enantioseparation is controlled by XB in an enthalpy-driven process ($\Delta\Delta S^\circ = -1.91$, $Q = 1.15$; EEO = S -
441 R). On the basis of the proposed model, as expected, by changing CDMPC to CDCPC (Fig. 6), an
442 increase of the enantioseparation for the fluorinated compound ($\alpha_{CDMPC} = 1.06 \rightarrow \alpha_{CDCPC} = 1.09$), and a
443 decrease for the brominated system were observed ($\alpha_{CDMPC} = 1.16 \rightarrow \alpha_{CDCPC} = 1.00$) due to the higher
444 acidity of the NH and the higher $V_{S,\min}$ value associated with the carbonyl oxygens in the chlorinated
445 selector ($V_{S,\min} (CDMPC) = -0.0625 \text{ au} \rightarrow V_{S,\min} (CDCPC) = -0.0536 \text{ au}$). By using mixture B as MP,

446 the enantioseparation of compounds **2**, like compound **1**, is driven by the N–H···Cl–Fc interaction and,
447 coherently, the EEO was *R-S* in both cases (Fig. 6). The EEO reversal in the enantioseparation of
448 compound **1** observed upon changing C-1 to iC-5 could be rationalized through the interplay between
449 the HB involving fluorine and the selector amidic hydrogen, and XB involving I as XB donor and the
450 selector carbonyl oxygen. Given the lower XB acceptor power of the carbonyl oxygens in the CDCPC of
451 iC-5, the XB is suppressed and the overall mechanism underlying retention and selectivity, and
452 consequently EEO, changes. This mechanism does not occur within the series **4-6**, and only enthalpic
453 thermodynamic profiles were derived in these cases.

454 Finally, the SF reconstruction of the V was applied to the $V_{S,max}$ and the $V_{S,min}$ associated with the
455 halogen (F, Cl, Br) σ -holes and negative belts of compounds **1-3**. The reconstruction of the $V_{S,max}$ related
456 to the iodine σ -hole (Fig. 7a) confirmed that no relevant differences in the atomic and group
457 contributions from the components of the molecules occurred in compounds **1-3**. In particular, the
458 decrease of the negative contribution from the distinctive halogen (green) was compensated by the
459 decrease of the positive contribution from the substituted Cp (orange), resulting in a similar negative
460 contribution from the Cp_{sub-X} groups to the $V_{S,max}$ ($SF(X) + SF(substituted\ Cp) = -0.0163$ au (**1**), -0.0173
461 au (**2**), -0.0175 au (**3**)) in all three cases. This analysis confirmed that the differences in the interaction
462 modes within compounds **1-3** cannot be ascribed to the iodine σ -holes. On the contrary, different
463 patterns could be observed for the SF reconstruction of the $V_{S,max}$ and the $V_{S,min}$ associated with the
464 distinctive halogen σ -holes (Fig. 7b) and negative belts (Fig. 7c). In particular, the Cp_{sub-X} group
465 contributed to the negative $V_{S,max}$ of the fluorine atom in **1** ($SF(X) + SF(substituted\ Cp) = -0.0638$ au),
466 whereas it opposes to the positive $V_{S,max}$ in **2** ($SF(X) + SF(substituted\ Cp) = -0.0153$ au) more than in **3**
467 ($SF(X) + SF(substituted\ Cp) = -0.0033$ au), resulting in the more positive $V_{S,max}$ for the bromine atom
468 compared to the chlorine atom. On the other hand, the $SF(Cp_{sub+X})$ contribution to the $V_{S,min}$ associated
469 with the negative belt of the corresponding halogen increases following the order F (-0.0655 au) > Cl ($-$
470 0.0633 au) > Br (-0.0625 au). In conclusion, for compounds **1-3** the comparison of the reconstruction

471 results confirmed the SF origins of the electronic properties, described in terms of $V_{S,max}$ and $V_{S,min}$,
472 which allowed for the rationalization of the enantioseparation mechanism as correlated with the
473 experimental results.

474 **4. Conclusions**

475 In the enantioseparation of halogenated ferrocenes **1-11** on polysaccharide-based CSPs, retention and
476 selectivity depend on a subtle balance between all possible functions and noncovalent interactions that
477 the distinctive halogens may carry out and forms, respectively. Despite the fact that the presence of
478 halogen atoms in a molecule increases its lipophilicity and hydrophobicity, halogens can also participate
479 in polar noncovalent interactions, under HPLC multimodal elution conditions. Thus, in principle, HB-
480 and XB-based, hydrophobic and repulsive interaction modes can be switched on, switched off, or finely
481 modulated depending on the structural features of analytes, halogens, CSPs, and MP polarity. As a
482 result, in the enantioseparation of planar chiral halogenated ferrocenes, boundaries conditions have to be
483 carefully selected as a function of halogen type and position in order to improve enantioseparation.

484 On this basis, the following practical guidelines can be provided to approach the enantioseparation of
485 halogenated ferrocenes on polysaccharide-based CSPs: *a)* methylated and chloromethylated amylose-
486 based columns exhibit better performances compared to cellulose-based columns; *b)* the rate of baseline
487 enantioseparation of the immobilized iA-1 is lower compared to the coated A-1; *c)* temperature can be
488 used as a parameter to optimize enantioseparation; *d)* methanol-containing mixtures provide better
489 results in term of selectivity factors compared to classical *n*-hexane-2-propanol mixtures.

490 In most cases, retention followed the order $F < Cl < Br$ which could be determined by the
491 electrophilic σ -hole on the halogen atoms under NP conditions, as well as by hydrophobic contacts
492 favoured in aqueous mixtures. However, it has been demonstrated that water may have little influence
493 on the interaction energies and geometries of XB adducts in solution [54]. Consequently, XB can be
494 considered as a hydrophobic equivalent of the hydrophilic HB [55], potentially also acting in water-
495 containing MPs [28].

496 Thermodynamic profiles and EEO reversal dependent on halogen type were observed on CDMPC as
497 selector. This phenomenon was explored at the molecular level by correlating experimental and
498 computational data, and for this purpose, theoretical approaches such as *V* analyses and related SF
499 reconstruction were successfully applied. Despite the fact that recognition mechanisms involving
500 multiple noncovalent interactions may be challenging to deconvolute, integrating experimental and
501 computational analysis represents a powerful tool to unravel the bases of enantioseparation mechanisms
502 at the molecular level.

503 **Acknowledgements**

504 We thank the Consiglio Nazionale delle Ricerche and the International Center Frontier Research in
505 Chemistry (icFRC) and the Laboratory of Excellence for Complex System Chemistry (LabEx CSC).

506 **Appendix A. Supplementary data**

507 Supplementary data associated with this article can be found, in the online version, at doi:

508 **References**

- 509 [1] T.J. Kealy, P.L. Pauson, A new type of organo-iron compound, *Nature* 168 (1951) 1039–1040.
510 DOI: 10.1038/1681039b0
- 511 [2] S.A. Miller, J.A. Tebboth, J.F. Tremaine, 114. Dicyclopentadienyliron, *J. Chem. Soc.* (1952) 632–
512 635. DOI: 10.1039/JR9520000632
- 513 [3] G. Wilkinson, M. Rosenblum, M.C. Whiting, R.B. Woodward, The structure of iron bis-
514 cyclopentadienyl, *J. Am. Chem. Soc.* 74 (1952) 2125–2126. DOI:10.1021/ja01128a527
- 515 [4] E.O. Fischer, W. Pfab, Zur Kristallstruktur der Di-Cyclopentadienyl-Verbindungen des
516 zweiwertigen Eisens, Kobalts und Nickels (On the crystal structure of the bis-cyclopentadienyl
517 compounds of divalent iron, cobalt and nickel), *Z. Naturforsch. B.* 7 (1952) 377–379. DOI:
518 10.1515/znb-1952-0701
- 519 [5] P.F. Eilan, R. Pepinsky, X-ray examination of iron biscyclopentadienyl, *J. Am. Chem. Soc.* 74
520 (1952) 4971. DOI: 10.1021/ja01139a527

- 521 [6] D. Astruc, Why is ferrocene so exceptional? *Eur. J. Inorg. Chem.* (2017) 6–29. DOI:
522 10.1002/ejic.201600983
- 523 [7] M. Patra, G. Gasser, The medicinal chemistry of ferrocene and its derivatives, *Nat. Rev. Chem.* 1
524 (2017) 0066. DOI: 10.1038/s41570-017-0066
- 525 [8] L. Cunningham, A. Benson, P.J. Guiry, Recent developments in the synthesis and applications of
526 chiral ferrocene ligands and organocatalysts in asymmetric catalysis, *Org. Biomol. Chem.* 18
527 (2020) 9329–9370. DOI: 10.1039/d0ob01933j
- 528 [9] A.N. Nesmeyanov, V.A. Sazonova, V.N. Drosd, Synthese von Ferrocenderivaten mittels bor- und
529 halogensubstituierter Ferrocene, *Chem. Ber.* 93 (1960) 2717–2729. DOI:
530 10.1002/cber.19600931143
- 531 [10] J.W. Huffman, J.F. Cope, Reactions of 2-methylchloroferrocene. Evidence for the ferrocene
532 intermediate, *J. Org. Chem.* 36 (1971) 4068–4072. DOI: 10.1021/jo00825a013
- 533 [11] W.R. Cullen, S.J. Rettig, T.C. Zheng, Ferrocene and ferrocene. Preparation and structures of
534 $\text{Os}_3(\text{CO})_9[\mu_3\text{-(C}_5\text{H}_3\text{)Fe(C}_5\text{H}_5\text{)}][\mu_3\text{-P(C}_5\text{H}_4\text{)Fe(C}_5\text{H}_5\text{)}]$, $\text{Os}_3(\text{H})_2(\text{CO})_8(\text{PPr}^i_2\text{C}_5\text{H}_2)\text{Fe(C}_5\text{H}_2\text{PPr}^i_2)\text{Os}_3$
535 $(\text{H})_2(\text{CO})_8$, and $\text{Os}_3(\text{CO})_9[\mu_3\text{-C}_6\text{H}_4][\mu_3\text{-P(C}_5\text{H}_4\text{)Fe(C}_5\text{H}_5\text{)}]$, *Organometallics* 11 (1992) 928–935.
536 DOI: 10.1021/om00038a064
- 537 [12] H. Butenschön, Haloferrocenes: syntheses and selected reactions, *Synthesis* 50 (2018) 3787–3808.
538 DOI: 10.1055/s-0037-1610210
- 539 [13] E. Aubert, A. Doudouh, E. Wenger, B. Sechi, P. Peluso, P. Pale, V. Mamane, Chiral ferrocenyl-
540 iodotriazoles and -iodotriazoliums as halogen bond donors. Synthesis, solid state analysis and
541 catalytic properties, *Eur. J. Inorg. Chem.* (2022) e202100927. DOI: 10.1002/ejic.202100927
- 542 [14] M. Wen, W. Erb, F. Mongin, Y.S. Halauko, O.A. Ivashkevich, V.E. Matulis, T. Roisnel, Synthesis
543 of polysubstituted ferrocenesulfoxides, *Molecules* 27 (2022) 1798. DOI:
544 10.3390/molecules27061798

- 545 [15] V. Mamane, P. Peluso, E. Aubert, R. Weiss, E. Wenger, S. Cossu, P. Pale, Disubstituted
546 ferrocenyl iodo- and chalcogenoalkynes as chiral halogen and chalcogen bond donors,
547 *Organometallics* 39 (2020) 3936–3950. DOI: 10.1021/acs.organomet.0c00633
- 548 [16] L.–X. Dai, T. Tu, S.–L. You, W.–P. Deng, X.–L. Hou, Asymmetric catalysis with chiral ferrocene
549 ligands, *Acc. Chem. Res.* 36 (2003) 659–667. DOI: 10.1021/ar020153m
- 550 [17] O. Riant, G. Argouarch, D. Guillaneux, O. Samuel, H.B. Kagan, A straightforward asymmetric
551 synthesis of enantiopure 1,2-disubstituted ferrocenes, *J. Org. Chem.* 63 (1998) 3511–3514. DOI:
552 10.1021/jo9800614
- 553 [18] F. Rebière, O. Riant, L. Ricard, H.B. Kagan, Asymmetric synthesis and highly diastereoselective
554 ortho-lithiation of ferrocenyl sulfoxides. Application to the synthesis of ferrocenyl derivatives with
555 planar chirality, *Angew. Chem. Int. Ed. Engl.* 32 (1993) 568–570. DOI: 10.1002/anie.199305681
- 556 [19] R.A. Thorat, S. Jain, M. Sattar, P. Yadav, Y. Mandhar, S. Kumar, Synthesis of chiral-substituted
557 2-aryl-ferrocenes by the Catellani reaction, *J. Org. Chem.* 85 (2020) 14866–14878. DOI:
558 10.1021/acs.joc.0c01360
- 559 [20] M. Tsukazaki, M. Tinkl, A. Roglans, B.J. Chapell, N.J. Taylor, V. Snieckus, Direct and highly
560 enantioselective synthesis of ferrocenes with planar chirality by (-)-sparteine-mediated lithiation, *J.*
561 *Am. Chem. Soc.* 118 (1996) 685–686. DOI: /10.1021/ja953246q
- 562 [21] W. Erb, M. Wen, J. P. Hurvois, F. Mongin, Y.S. Halauko, O.A. Ivashkevich, V.E. Matulis, T.
563 Roisnel, *O*-Isopropylferrocenesulfonate: synthesis of polysubstituted derivatives and
564 electrochemical study, *Eur. J. Inorg. Chem.* (2021) 3165–3176. DOI: 10.1002/ejic.202100448
- 565 [22] Y. Yamazaki, N. Morohashi, K. Hosono, High-performance liquid chromatographic determination
566 of optical purity of planar chiral organometallic compounds resolved by enzymic transformations,
567 *J. Chromatogr. A* 542 (1991) 129–136. DOI: 10.1016/S0021-9673(01)88753-7

- 568 [23] A. Patti, S. Pedotti, C. Sanfilippo, Comparative HPLC enantioseparation of ferrocenylalcohols on
569 two cellulose-based chiral stationary phases, *Chirality* 19 (2007) 344-351. DOI:
570 10.1002/chir.20386
- 571 [24] M. Ogasawara, Y. Enomoto, M. Uryu, X. Yang, A. Kataoka, A. Ohnishi, Application of
572 polysaccharide-based chiral HPLC columns for separation of nonenantiomeric isomeric mixtures
573 of organometallic compounds, *Organometallics* 38 (2019) 512–518. DOI:
574 10.1021/acs.organomet.8b00819
- 575 [25] A. Dessì, B. Sechi, R. Dallochio, B. Chankvetadze, M. Pérez-Baeza, S. Cossu, V. Mamane, P.
576 Pale, P. Peluso, Comparative enantioseparation of planar chiral ferrocenes on polysaccharide-
577 based chiral stationary phases, *Chirality* 34 (2022) 609–619. DOI: 10.1002/chir.23417
- 578 [26] P. Peluso, V. Mamane, S. Cossu, Liquid chromatography enantioseparations of halogenated
579 compounds on polysaccharide-based chiral stationary phases: role of halogen substituents in
580 molecular recognition. *Chirality* 27 (2015), 667–684. DOI: 10.1002/chir.22485
- 581 [27] P. Peluso, V. Mamane, E. Aubert, A. Dessì, R. Dallochio, A. Dore, P. Pale, S. Cossu, Insights
582 into halogen bond-driven enantioseparations, *J. Chromatogr. A* 1467 (2016) 228–238. DOI:
583 10.1016/j.chroma.2016.06.007
- 584 [28] P. Peluso, V. Mamane, R. Dallochio, A. Dessì, R. Villano, D. Sanna, E. Aubert, P. Pale, S.
585 Cossu, Polysaccharide-based chiral stationary phases as halogen bond acceptors: A novel strategy
586 for detection of stereoselective σ -hole bonds in solution, *J. Sep. Sci.* 41 (2018) 1247–1256. DOI:
587 10.1002/jssc.201701206
- 588 [29] P. Peluso, B. Chankvetadze, The molecular bases of chiral recognition in 2-
589 (benzylsulfinyl)benzamide enantioseparation, *Anal. Chim. Acta* 1141 (2021) 194–205. DOI:
590 10.1016/j.aca.2020.10.050

- 591 [30] C. Gatti, The source function descriptor as a tool to extract chemical information from theoretical
592 and experimental electron densities, *Struct. Bond.* 147 (2012) 193–286. DOI:
593 10.1007/430_2010_31
- 594 [31] C. Gatti, A. Dessì, R. Dallochio, V. Mamane, S. Cossu, R. Weiss, P. Pale, E. Aubert, P. Peluso,
595 Factors impacting σ - and π -hole regions as revealed by the electrostatic potential and its source
596 function reconstruction: The case of 4,4'-bipyridine derivatives, *Molecules* 25 (2020) 4409. DOI:
597 10.3390/molecules25194409
- 598 [32] P. Peluso, A. Dessì, R. Dallochio, B. Sechi, C. Gatti, B. Chankvetadze, V. Mamane, R. Weiss, P.
599 Pale, E. Aubert, S. Cossu, Enantioseparation of 5,5'-dibromo-2,2'-dichloro-3-selanyl-4,4'-
600 bipyridines on polysaccharide-based chiral stationary phases: exploring chalcogen bonds in liquid-
601 phase chromatography, *Molecules* 26 (2021) 221. DOI: 10.3390/molecules26010221
- 602 [33] P. Peluso, C. Gatti, A. Dessì, R. Dallochio, R. Weiss, E. Aubert, P. Pale, S. Cossu, V. Mamane,
603 Enantioseparation of fluorinated 3-arylthio-4,4'-bipyridines: insights into chalcogen and π -hole
604 bonds in high-performance liquid chromatography, *J. Chromatogr. A* 1567 (2018) 119–129. DOI:
605 10.1016/j.chroma.2018.06.060
- 606 [34] M. Tazi, M. Hedidi, W. Erb, Y.S. Halauko, O.A. Ivashkevich, V.E. Matulis, T. Roisnel, V. Dorcet,
607 G. Bentabed-Ababsa, F. Mongin, Fluoro- and chloroferrocene: from 2- to 3-substituted
608 derivatives, *Organometallics* 37 (2018) 2207–221. DOI: 10.1021/acs.organomet.8b00384
- 609 [35] M. Tazi, W. Erb, T. Roisnel, V. Dorcet, F. Mongin, P.J. Low, From ferrocene to fluorine-
610 containing pentasubstituted derivatives and all points in-between; or, how to increase the available
611 chemical space, *Org. Biomol. Chem.* 17 (2019) 9352–9359. DOI: 10.1039/c9ob01885a
- 612 [36] G. Dayaker, A. Sreeshailam, F. Chevallier, T. Roisnel, P.R. Krishna, F. Mongin, Deprotonative
613 metallation of ferrocenes using mixed lithium–zinc and lithium–cadmium combinations, *Chem.*
614 *Commun.* 46 (2010) 2862–2864. DOI: 10.1039/B924939G

- 615 [37] M.J. Frisch, G.W. Trucks, H.B. Schlegel, G.E. Scuseria, M.A. Robb, J.R. Cheeseman, G.
616 Scalmani, V. Barone, B. Mennucci, G.A. Petersson, H. Nakatsuji, M. Caricato, X. Hratchian, H.P.
617 Li, A.F. Izmaylov, J. Bloino, G. Zheng, J.L. Sonnenberg, M. Hada, M. Ehara, K. Toyota, R.
618 Fukuda, J. Hasegawa, M. Ishida, T. Nakajima, Y. Honda, O. Kitao, H. Nakai, T. Vreven, J.A.
619 Montgomery Jr., J.E. Peralta, F. Ogliaro, M. Bearpark, J.J. Heyd, E. Brothers, K.N. Kudin, V.N.
620 Staroverov, T. Keith, R. Kobayashi, J. Normand, K. Raghavachari, A. Rendell, J.C. Burant, S.S.
621 Iyengar, J. Tomasi, M. Cossi, N. Rega, J.M. Millam, M. Klene, J.E. Knox, J.B. Cross, V. Bakken,
622 C. Adamo, J. Jaramillo, R. Gomperts, R.E. Stratmann, O. Yazyev, A.J. Austin, R. Cammi, C.
623 Pomelli, J.W. Ochterski, R.L. Martin, K. Morokuma, V.G. Zakrzewski, G. Voth, P. Salvador, J.J.
624 Dannenberg, S. Dapprich, A.D. Daniels, O. Farkas, J.B. Foresman, J. Ortiz, J. Cioslowski, D.J.
625 Fox, Gaussian 09, Revision B. 01, Inc. Gaussian, C.T. Wallingford, 2010.
- 626 [38] T. Lu, F. Chen, Multiwfn: A multifunctional wavefunction analyser. *J. Comp. Chem.* 33 (2012)
627 580–592. DOI: 10.1002/jcc.22885
- 628 [39] T. Lu, F. Chen, Quantitative analysis of molecular surface based on improved Marching
629 Tetrahedra algorithm. *J. Mol. Graph. Model.* 38 (2012) 314–323. DOI:
630 10.1016/j.jm gm.2012.07.004
- 631 [40] B. Chankvetadze, Recent trends in preparation, investigation and application of polysaccharide-
632 based chiral stationary phases for separation of enantiomers in high-performance liquid
633 chromatography, *Trends Anal. Chem.* 122 (2020) 115709. DOI: 10.1016/j.trac.2019.115709
- 634 [41] P. Peluso, B. Sechi, G. Lai, A. Dessì, R. Dallochio, S. Cossu, E. Aubert, R. Weiss, P. Pale, V.
635 Mamane, B. Chankvetadze, Comparative enantioseparation of chiral 4,4'-bipyridine derivatives on
636 coated and immobilized amylose-based chiral stationary phases, *J. Chromatogr. A.* 1625 (2020)
637 461303. DOI: 10.1016/j.chroma.2020.461303
- 638 [42] B. Chankvetadze, C. Yamamoto, Y. Okamoto, Enantioseparation of selected chiral sulfoxides
639 using polysaccharide-type chiral stationary phases and polar organic, polar aqueous–organic and

- 640 normal-phase eluents, *J. Chromatogr. A.* 922 (2001) 127–137. DOI: 10.1016/S0021-
641 9673(01)00958-X
- 642 [43] B. Chankvetadze, Recent developments on polysaccharide-based chiral stationary phases for
643 liquid-phase separation of enantiomers, *J. Chromatogr. A.* 1269 (2012) 26–51. DOI:
644 10.1016/j.chroma.2012.10.033
- 645 [44] M. Dobó, M. Foroughbakhshfasaei, P. Horváth, Z.–I. Szabó, G. Tóth, Chiral separation of
646 oxazolidinone analogues by liquid chromatography on polysaccharide stationary phases using
647 polar organic mode, *J. Chromatogr. A.* 1662 (2022) 462741. DOI: 10.1016/j.chroma.2021.462741
- 648 [45] Z. Shedania, R. Kakava, A. Volonterio, T. Farkas, B. Chankvetadze, Separation of enantiomers of
649 chiral sulfoxides in high-performance liquid chromatography with cellulose-based chiral selectors
650 using methanol and methanol-water mixtures as mobile phases, *J. Chromatogr. A.* 1557 (2018) 62–
651 74. DOI: 10.1016/j.chroma.2018.05.002
- 652 [46] A. Singh, I. Lumb, V. Mehra, V. Kumar, Ferrocene-appended pharmacophores: an exciting
653 approach for modulating the biological potential of organic scaffolds, *Dalton Trans.* 48 (2019)
654 2840–2860. DOI: 10.1039/c8dt03440k
- 655 [47] A. Bondi, van der Waals volume and radii, *J. Phys. Chem.* 68 (1964) 441–451. DOI:
656 10.1021/j100785a001
- 657 [48] C. Gatti, F. Cargnoni, L. Bertini, Chemical information from the source function, *J. Comput.*
658 *Chem.* 24 (2003) 422–436. DOI: 10.1002/jcc.10205
- 659 [49] I. Matarashvili, G. Kobidze, A. Chelidze, G. Dolidze, N. Beridze, G. Jibuti, T. Farkas, B.
660 Chankvetadze, The effect of temperature on the separation of enantiomers with coated and
661 covalently immobilized polysaccharide-based chiral stationary phases, *J. Chromatogr. A* 1599
662 (2019) 172–179. DOI: 10.1016/j.chroma.2019.04.024
- 663 [50] F. Ianni, Z. Pataj, H. Gross, R. Sardella, B. Natalini, W. Lindner, M. Lämmerhofer, Direct
664 enantioseparation of underivatized aliphatic 3-hydroxyalkanoic acids with a quinine-based

665 zwitterionic chiral stationary phase, *J. Chromatogr. A* 1363 (2014) 101–108. DOI:
666 10.1016/j.chroma.2014.03.060

667 [51] P. Peluso, V. Mamane, R. Dallochio, A. Dessì, S. Cossu, Noncovalent interactions in high-
668 performance liquid chromatography enantioseparations on polysaccharide-based chiral selectors, *J.*
669 *Chromatogr. A* 1623 (2020) 461202. DOI: 1016/j.chroma.2020.461202.

670 [52] T. Fornstedt, Characterization of adsorption processes in analytical liquid–solid chromatography,
671 *J. Chromatogr. A* 1217 (2010) 792–812. DOI: 10.1016/j.chroma.2009.12.044

672 [53] D. Tanács, T. Orosz, Z. Szakonyi, T.M. Le, F. Fülöp, W. Lindner, I. Ilisz, A. Péter, High-
673 performance liquid chromatographic enantioseparation of isopulegol-based β -amino lactone and β -
674 amino amide analogs on polysaccharide-based chiral stationary phases focusing on the change of
675 the enantiomer elution order, *J. Chromatogr. A* 1621 (2020) 461054. DOI:
676 10.1016/j.chroma.2020.461054

677 [54] Y. Lu, H. Li, X. Zhu, W. Zhu, H. Liu, How does halogen bonding behave in solution? A
678 theoretical study using implicit solvation model, *J. Phys. Chem. A* 115 (2011) 4467–4475. DOI:
679 10.1021/jp111616x

680 [55] A. Priimagi, G. Cavallo, P. Metrangolo, G. Resnati, The halogen bond in the design of functional
681 supramolecular materials: recent advances, *Acc. Chem. Res.* 46 (2013) 2686–2695. DOI:
682 10.1021/ar400103r

683

684

685 **FIGURE CAPTIONS**

686 **Fig. 1.** Structures and numbering of halogenated chiral ferrocenes **1-11**.

687 **Fig. 2.** V isosurface (0.002 au) of compound **2**, as a representative analyte, showing the main interaction
688 sites of the molecular systems featuring compounds **1-11** (colour legend: red, high electron charge
689 density regions; blue, regions of electron charge density depletion; pale blue, green, yellow, and orange
690 describes intermediate regions of electron charge density between the two extrema (red and blue
691 regions).

692 **Fig. 3.** Comparison of retention factor of the first eluted enantiomers (k_1) of compounds **1-11** on chiral
693 columns C-1 (a, d, g, j), A-1 (b, e, h, k), and iA-3 (c, f, i, l) under multimodal elution conditions (A,
694 Hex/2-PrOH 95:5 v/v; B, Hex/2-PrOH/MeOH 95:2.5:2.5 v/v/v; C, MeOH 100%; D, MeOH/water 95:5
695 v/v; E, MeOH/water 90:10 v/v).

696 **Fig. 4.** Comparison of selectivity factors (α) of compounds **1-11** on chiral columns C-1 (a, d, g, j), A-1
697 (b, e, h, k), and iA-3 (c, f, i, l) under multimodal elution conditions (A, Hex/2-PrOH 95:5 v/v; B, Hex/2-
698 PrOH/MeOH 95:2.5:2.5 v/v/v; C, MeOH 100%; D, MeOH/water 95:5 v/v; E, MeOH/water 90:10 v/v).

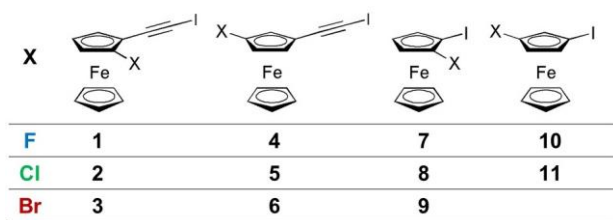
699 **Fig. 5.** Enantioseparation of compounds **1** (a), **2** (b), and **3** (c) at variable temperature on C-1 with
700 mixture A, and variation of the $V_{S,\min}$ and $V_{S,\max}$ values as the 1-halogen substituent changes in the series
701 of 1-halo-2-(iodoethynyl)ferrocenes **1-3**.

702 **Fig. 6.** Comparative enantioseparation of compounds **1** (a), **2** (b), and **3** (c) ($T = 25^\circ\text{C}$) by using the
703 chromatographic system C-1/A (blue), iC-5/A (red), and C-1/B (green).

704 **Fig. 7.** Iodine σ -hole $V_{S,\max}$ (a), and halogen ($X = \text{F, Cl, Br}$) $V_{S,\max}$ (b) and $V_{S,\min}$ (c) Source Function
705 reconstruction for compounds **1**, **2**, and **3** (see Supplementary data, Tables S4-S12 for complete data).

706

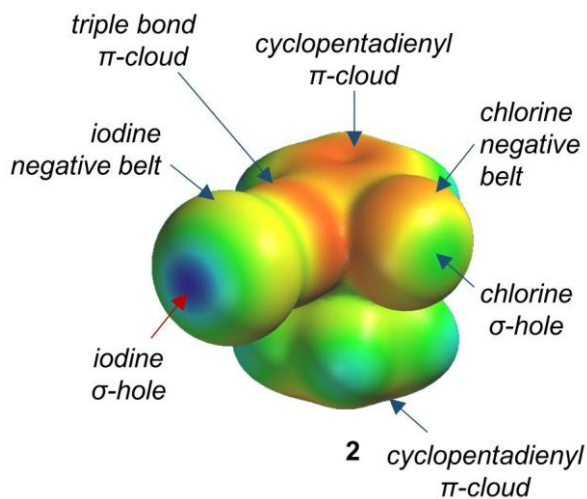
707



708

709 **Fig. 1.** Structures and numbering of halogenated chiral ferrocenes **1-11**.

710



711

712 **Fig. 2.** *V* isosurface (0.002 au) of compound **2**, as a representative analyte, showing the main interaction

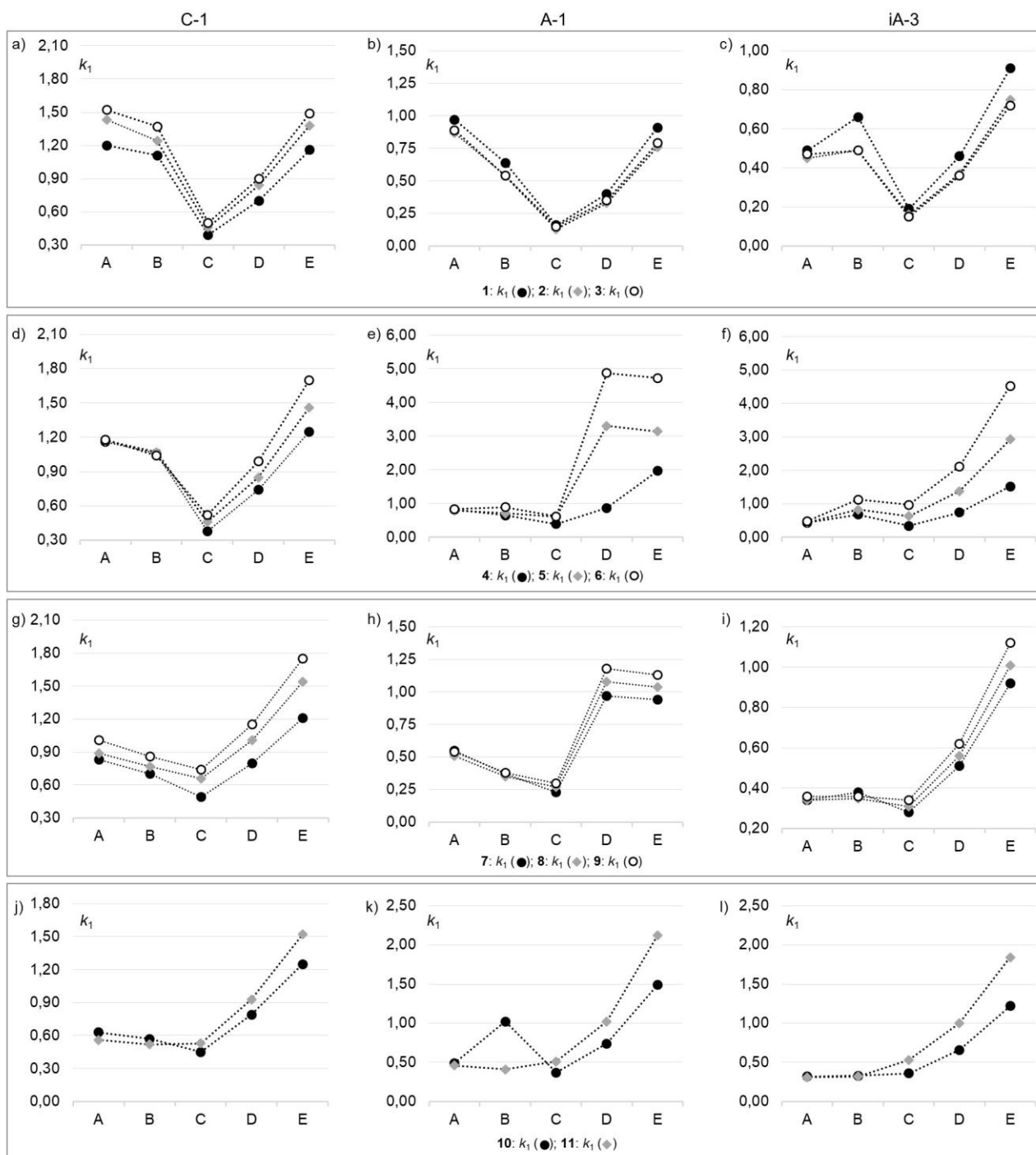
713 sites of the molecular systems featuring compounds **1-11** (colour legend: red, high electron charge

714 density regions; blue, regions of electron charge density depletion; pale blue, green, yellow, and orange

715 describes intermediate regions of electron charge density between the two extrema (red and blue

716 regions).

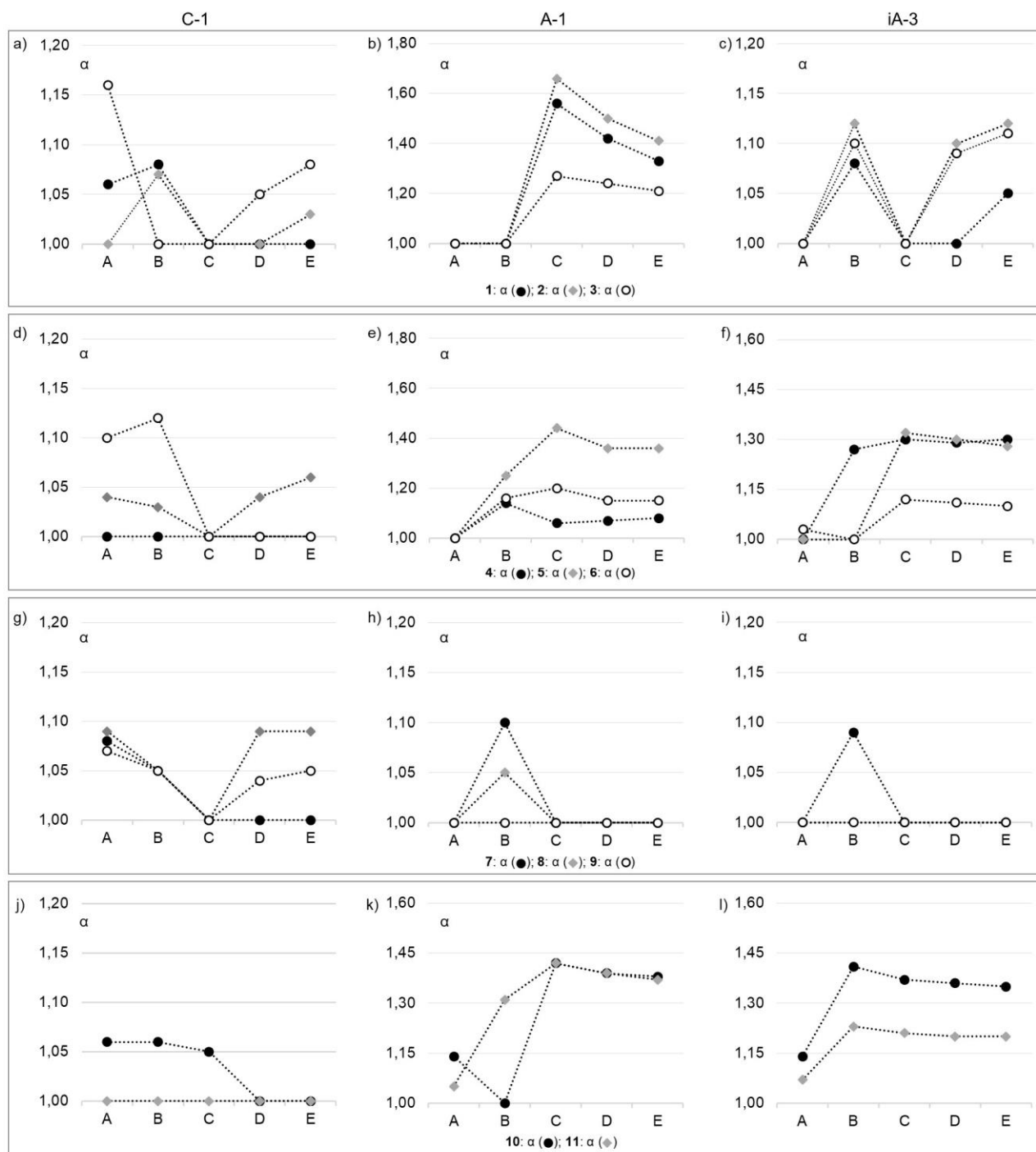
717



718

719 **Fig. 3.** Comparison of retention factor of the first eluted enantiomers (k_1) of compounds **1-11** on chiral
 720 columns C-1 (a, d, g, j), A-1 (b, e, h, k), and iA-3 (c, f, i, l) under multimodal elution conditions (A,
 721 Hex/2-PrOH 95:5 v/v; B, Hex/2-PrOH/MeOH 95:2.5:2.5 v/v/v; C, MeOH 100%; D, MeOH/water 95:5
 722 v/v; E, MeOH/water 90:10 v/v).

723

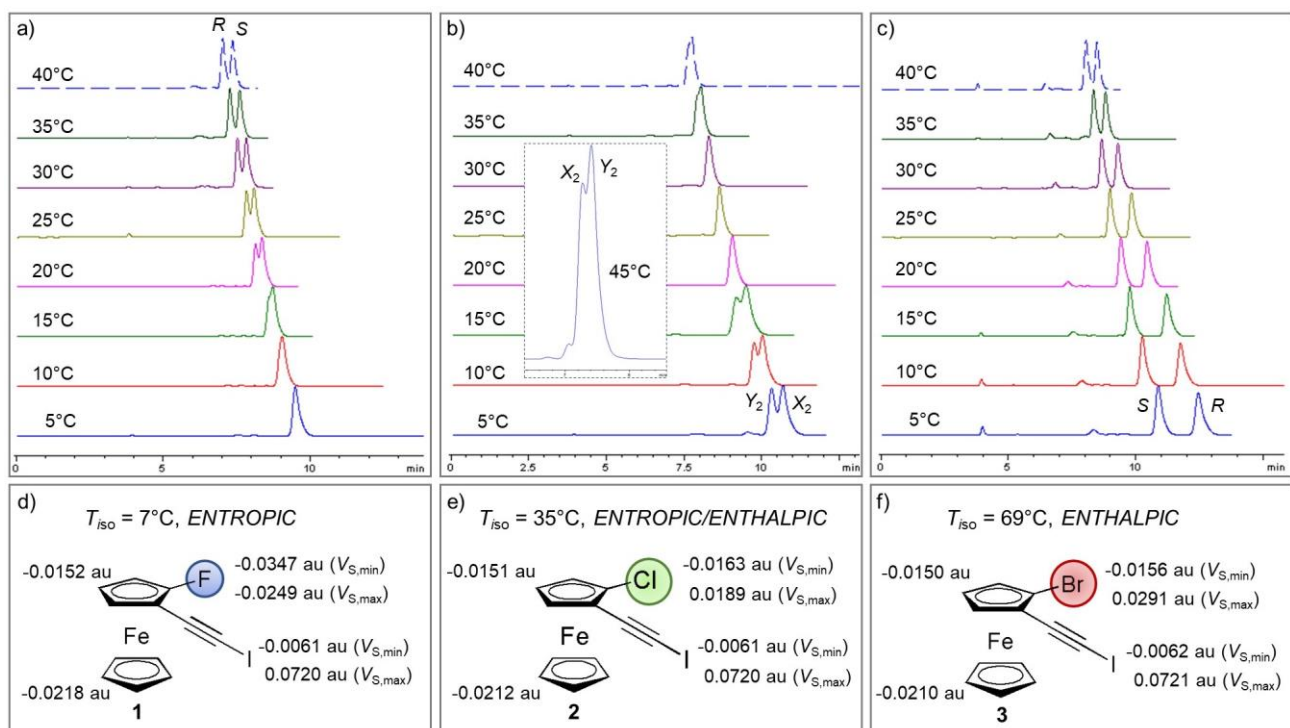


724

725 **Fig. 4.** Comparison of selectivity factors (α) of compounds **1-11** on chiral columns C-1 (a, d, g, j), A-1
 726 (b, e, h, k), and iA-3 (c, f, i, l) under multimodal elution conditions (A, Hex/2-PrOH 95:5 v/v; B, Hex/2-
 727 PrOH/MeOH 95:2.5:2.5 v/v/v; C, MeOH 100%; D, MeOH/water 95:5 v/v; E, MeOH/water 90:10 v/v).

728

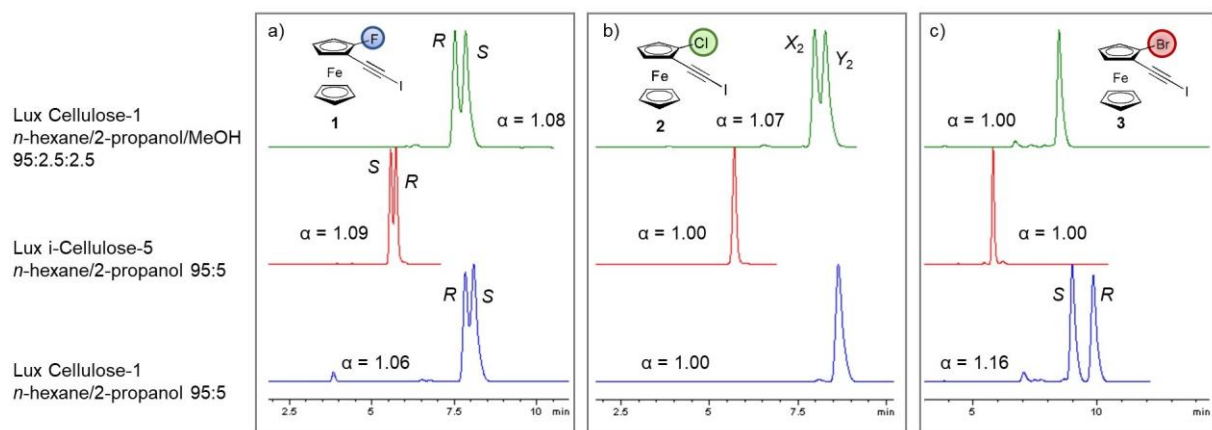
729



730

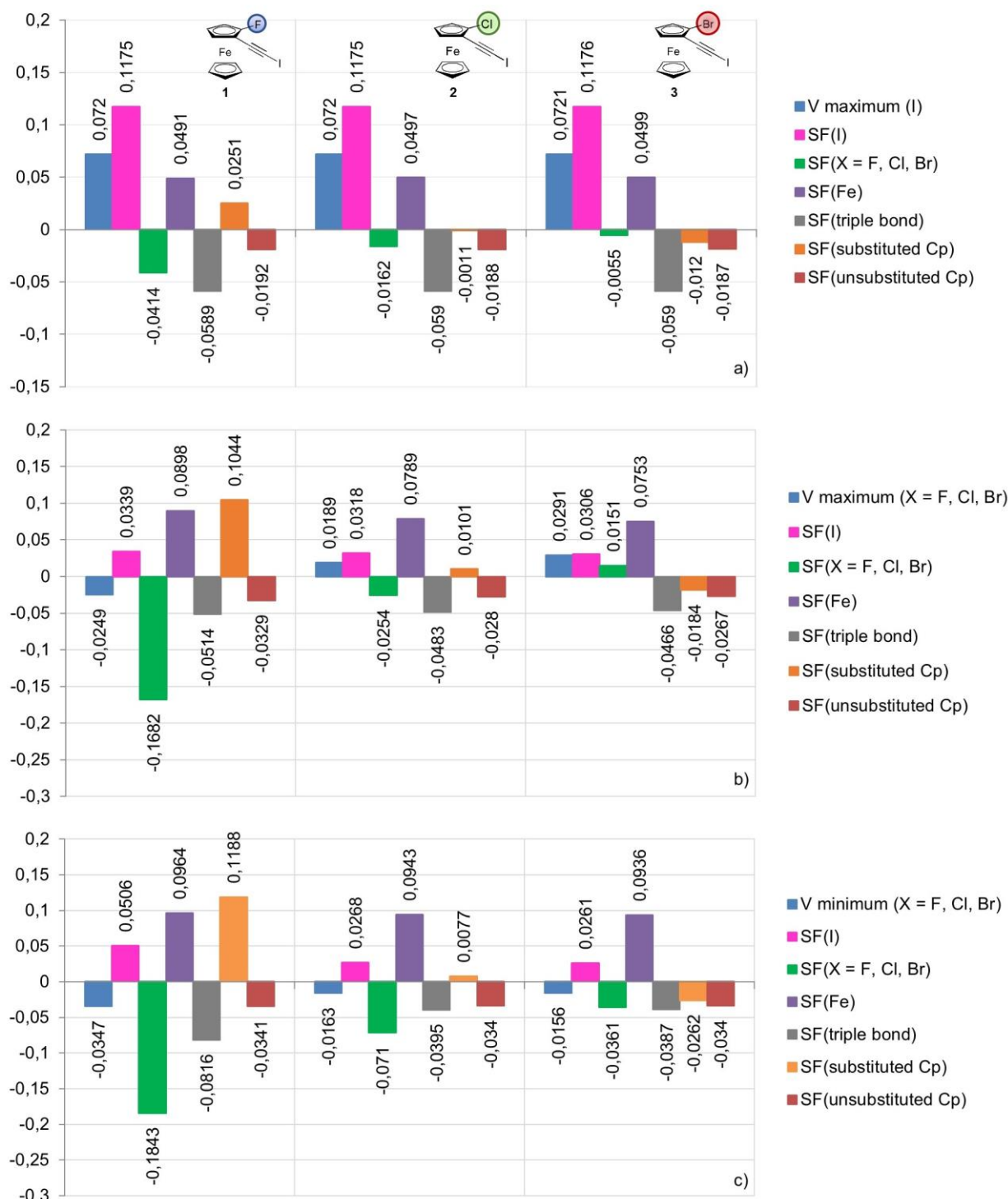
731 **Fig. 5.** Enantioseparation of compounds **1** (a), **2** (b), and **3** (c) at variable temperature on C-1 with
 732 mixture A, and variation of the $V_{S,min}$ and $V_{S,max}$ values as the 1-halogen substituent changes in the series
 733 of 1-halo-2-(iodoethyl)ferrocenes **1-3** (d-f).

734



735

736 **Fig. 6.** Comparative enantioseparation of compounds **1** (a), **2** (b), and **3** (c) ($T = 25^\circ\text{C}$) by using the
 737 chromatographic system C-1/A (blue), iC-5/A (red), and C-1/B (green).



738

739 **Fig. 7.** Iodine σ -hole $V_{S,max}$ (a), and halogen (X = F, Cl, Br) $V_{S,max}$ (b) and $V_{S,min}$ (c) Source Function740 reconstruction for compounds **1**, **2**, and **3** (see Supplementary data, Tables S4-S12 for complete data).

741

Table 1. Enantiomer elution orders (EEOs) determined for all enantioseparations of compounds **1-11** (25°C). EEOs reported in red were derived by chromatographic correlation (see text).

MP	CSP	F 1	Cl 2	Br 3	F 4	Cl 5	Br 6	F 7	Cl 8	Br 9	F 10	Cl 11
A	C-1	<i>R-S</i>	--	<i>S-R</i>	--	<i>X₅-Y₅</i>	<i>S-R</i>	<i>X₇-Y₇</i>	<i>X₈-Y₈</i>	<i>X₉-Y₉</i>	<i>X₁₀-Y₁₀</i>	--
	iC-5	<i>S-R</i>	--	--	--	--	--	--	--	--	--	--
	A-1	--	--	--	--	--	--	--	--	--	<i>X₁₀-Y₁₀</i>	<i>X₁₁-Y₁₁</i>
	iA-1	--	--	--	--	--	--	<i>Y₇-X₇</i>	--	--	<i>X₁₀-Y₁₀</i>	<i>X₁₁-Y₁₁</i>
	iA-3	--	--	--	--	--	<i>S-R</i>	--	--	--	<i>X₁₀-Y₁₀</i>	<i>X₁₁-Y₁₁</i>
B	C-1	<i>R-S</i>	<i>X₂-Y₂ → R-S</i>	--	--	<i>X₅-Y₅</i>	<i>S-R</i>	<i>X₇-Y₇</i>	<i>X₈-Y₈</i>	<i>X₉-Y₉</i>	<i>X₁₀-Y₁₀</i>	--
	iC-5	<i>S-R</i>	--	--	--	--	--	--	--	--	--	--
	A-1	--	--	--	<i>X₄-Y₄</i>	<i>Y₅-X₅</i>	<i>R-S</i>	<i>Y₇-X₇</i>	<i>X₈-Y₈</i>	--	--	<i>X₁₁-Y₁₁</i>
	iA-1	--	--	--	<i>X₄-Y₄</i>	<i>Y₅-X₅</i>	--	<i>Y₇-X₇</i>	--	--	<i>X₁₀-Y₁₀</i>	<i>X₁₁-Y₁₁</i>
	iA-3	<i>R-S</i>	<i>X₂-Y₂ → R-S</i>	<i>R-S</i>	<i>X₄-Y₄</i>	--	--	<i>Y₇-X₇</i>	--	--	<i>X₁₀-Y₁₀</i>	<i>X₁₁-Y₁₁</i>
C	C-1	--	--	--	--	--	--	--	--	--	<i>X₁₀-Y₁₀</i>	--
	A-1	<i>S-R</i>	<i>Y₂-X₂ → S-R</i>	<i>S-R</i>	<i>X₄-Y₄</i>	<i>Y₅-X₅</i>	<i>R-S</i>	--	--	--	<i>X₁₀-Y₁₀</i>	<i>X₁₁-Y₁₁</i>
	iA-1	--	--	--	<i>X₄-Y₄</i>	<i>Y₅-X₅</i>	--	--	--	--	<i>X₁₀-Y₁₀</i>	<i>X₁₁-Y₁₁</i>
	iA-3	--	--	--	<i>X₄-Y₄</i>	<i>Y₅-X₅</i>	<i>R-S</i>	--	--	--	<i>X₁₀-Y₁₀</i>	<i>X₁₁-Y₁₁</i>
D	C-1	--	--	<i>S-R</i>	--	<i>Y₅-X₅</i>	--	--	<i>Y₈-X₈</i>	<i>Y₉-X₉</i>	--	--
	A-1	<i>S-R</i>	<i>Y₂-X₂ → S-R</i>	<i>S-R</i>	<i>X₄-Y₄</i>	<i>Y₅-X₅</i>	<i>R-S</i>	--	--	--	<i>X₁₀-Y₁₀</i>	<i>X₁₁-Y₁₁</i>
	iA-1	--	--	--	<i>X₄-Y₄</i>	<i>Y₅-X₅</i>	--	--	--	--	<i>X₁₀-Y₁₀</i>	<i>X₁₁-Y₁₁</i>
	iA-3	--	<i>X₂-Y₂ → R-S</i>	<i>R-S</i>	<i>X₄-Y₄</i>	<i>Y₅-X₅</i>	<i>R-S</i>	--	--	--	<i>X₁₀-Y₁₀</i>	<i>X₁₁-Y₁₁</i>
E	C-1	--	<i>Y₂-X₂ → S-R</i>	<i>S-R</i>	--	<i>Y₅-X₅</i>	--	--	<i>Y₈-X₈</i>	<i>Y₉-X₉</i>	--	--
	A-1	<i>S-R</i>	<i>Y₂-X₂ → S-R</i>	<i>S-R</i>	<i>X₄-Y₄</i>	<i>Y₅-X₅</i>	<i>R-S</i>	--	--	--	<i>X₁₀-Y₁₀</i>	<i>X₁₁-Y₁₁</i>
	iA-1	--	--	--	<i>X₄-Y₄</i>	<i>Y₅-X₅</i>	--	--	--	--	<i>X₁₀-Y₁₀</i>	<i>X₁₁-Y₁₁</i>
	iA-3	<i>R-S</i>	<i>X₂-Y₂ → R-S</i>	<i>R-S</i>	<i>X₄-Y₄</i>	<i>Y₅-X₅</i>	<i>R-S</i>	--	--	--	<i>X₁₀-Y₁₀</i>	<i>X₁₁-Y₁₁</i>